ACS APPLIED MATERIALS & INTERFACES

Research Article

www.acsami.org

Phase Transformation of Molecular Beam Epitaxy-Grown Nanometer-Thick Gd_2O_3 and Y_2O_3 on GaN

Wen-Hsin Chang,[†,⊥] Shao-Yun Wu,[†,⊥] Chih-Hsun Lee,[†] Te-Yang Lai,[†] Yi-Jun Lee,[†] Pen Chang,[†] Chia-Hung Hsu,*[,§] Tsung-Shiew Huang,[†] J. Raynien Kwo,[‡] and Minghwei Hong*[,∥]

[†]Department of Materials Science and Engineering and [‡]Department of Physics, National Tsing Hua University, Hsinchu 30013, Taiwan

[§]Scientific Research Division, National Synchrotron Radiation Research Center, Hsinchu 30076, Taiwan

[∥]Graduate Institute of Applied Physics and Department of Physics, National Taiwan University, Taipei 10617, Taiwan

ABSTRACT: High quality nanometer-thick Gd_2O_3 and Y_2O_3 (rare-earth oxide, R_2O_3) films have been epitaxially grown on GaN (0001) substrate by molecular beam epitaxy (MBE). The R_2O_3 epi-layers exhibit remarkable thermal stability at 1100 °C, uniformity, and highly structural perfection. Structural investigation was carried out by in situ reflection high energy electron diffraction (RHEED) and ex-situ X-ray diffraction (XRD) with synchrotron radiation. In the initial stage of epitaxial growth, the R_2O_3 layers have a hexagonal phase with the epitaxial relationship of R_2O_3 $(0001)_H\langle 11\bar{2}0\rangle_H$//GaN-$(0001)_H\langle 11\bar{2}0\rangle_H$. With the increase in R_2O_3 film thickness, the structure of the R_2O_3 films changes from single domain hexagonal phase to monoclinic phase with six different rotational domains, following the R_2O_3 $(\bar{2}01)_M[020]_M$//GaN$(0001)_H\langle 11\bar{2}0\rangle_H$ orientational relationship. The structural details and fingerprints of hexagonal and monoclinic phase Gd_2O_3 films have also been examined by using electron energy loss spectroscopy (EELS). Approximate 3−4 nm is the critical thickness for the structural phase transition depending on the composing rare earth element.

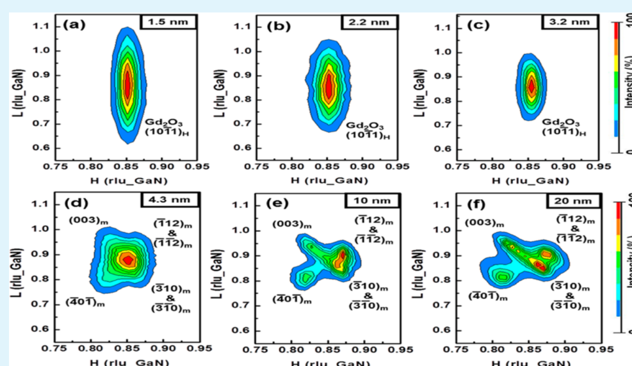

KEYWORDS: *phase transformation, monoclinic, hexagonal, GaN, Gd_2O_3, MBE*

■ INTRODUCTION

Heteroepitaxy between two dissimilar materials has been the key for producing artificial structured materials, the building blocks for new sciences, novel devices, and advanced technologies.[1−7] Particularly, the epitaxial growth among oxides and semiconductors has always been scientifically intriguing and technologically relevant.[3−8] One notable example is the successful growth of single crystal GaN on sapphire and Si(111), which has led to the recent commercialization of solid state lighting and the feverish research efforts on high power devices.[3−5] The growth of single crystal Gd_2O_3 on GaAs(001)[6] is another example, leading to the first demonstration of inversion-channel GaAs metal-oxide-semiconductor field-effect-transistors (MOSFETs),[9] timely for the ultimate complementary MOS (CMOS) technology.[10,11]

Rare earth oxides Gd_2O_3 and Y_2O_3 of cubic phase were found to grow epitaxially on Si, Ge, and GaAs. The lattice constants of cubic Gd_2O_3 and Y_2O_3 are 10.8 and 10.6 Å, respectively, which are approximately twice those of GaAs, Si, and Ge of being 5.65, 5.43, and 5.65 Å, respectively. The oxides deposited on the (111) oriented Si exhibit the same (111) surface normal.[12] Interestingly, the oxides deposited on the (001) oriented GaAs,[6] Si,[13] and Ge[14] have (011) parallel with the (001) normal of the semiconductors. The in-plane lattice spacing of the oxide (011) does not match well with those of GaAs,[15] Si,[13,16] and Ge,[17] indicating the bond arrangement and the energy consideration at the oxide/semiconductor interfaces may be more critical than the crystalline symmetry.

Besides the epitaxial growth, an effective passivation of high κ dielectrics on semiconductor has been intensively studied as higher device performance demands smaller device sizes and thinner gate dielectrics. GaN and its related compounds, which have been used for high-temperature high-power RF electronics because of the large critical breakdown fields and high saturation velocities,[18] are now being considered for the post Si CMOS technology. In the past few years, GaN MOSFETs have been demonstrated using MgO,[19,20] Al_2O_3,[21] HfO_2,[22] and $Ga_2O_3(Gd_2O_3)$[23] as the gate dielectrics. For pushing the GaN MOS technology, the equivalent oxide thickness (EOT) of the gate dielectric is required to be much less than 1 nm.[11] Therefore, the dielectric constant of the gate dielectric has to be enhanced. Moreover, self-aligned inversion-channel GaN

Received: November 28, 2012
Accepted: January 28, 2013
Published: January 29, 2013

© 2013 American Chemical Society

dx.doi.org/10.1021/am302881y | ACS Appl. Mater. Interfaces 2013, 5, 1436−1441

MOSFETs may require the gate dielectric to be of single crystal as amorphous films tend to form polycrystalline structures resulting from the high temperature source/drain (S/D) dopant activation process; the gate dielectric needs to sustain rapid thermal annealing (RTA) processes up to 1100 °C for at least 5 minutes.[24] High-quality hexagonal phase Gd_2O_3 with good crystallinity has been successfully deposited on *c*-plane GaN and shows excellent electrical properties.[25,26] More recently, the monoclinic Gd_2O_3 and Y_2O_3 layers consisting of six different rotational domains on GaN have also been reported.[27−29] The monoclinic phase of rare earth oxides is not energetically favorable under ambient conditions. The presence of these nonambient phases is attributed to epitaxial stabilization.

In this work, we have systematically scaled down the thickness of the molecular beam epitaxy (MBE) deposited Gd_2O_3 and Y_2O_3 on GaN from 20 to 10 nm to 1−2 nm. With decreasing layer thickness to 2−4 nm, the structure of the rare-earth oxides changes from monoclinic phase to hexagonal phase. There are great similarities on the structural properties between Gd_2O_3 and Y_2O_3. The discussion will, therefore, focus on Gd_2O_3. The structural characterizations were performed by high resolution X-ray diffraction (HRXRD) with synchrotron radiation. The electron energy loss spectroscopy (EELS) was employed to investigate structural fingerprints of different phases of Gd_2O_3.

EXPERIMENTAL SECTION

A 0.3 μm thick *n*-GaN layer with a doping of 5×10^{17} cm^{-3} and a 1.5 μm thick GaN buffer layer were grown on a 2-in. *c*-plane (0001) sapphire substrate by metal−organic chemical vapor deposition (MOCVD). The GaN surface was determined to be Ga-polar. Before oxide deposition, the GaN substrates were annealed to 650−700 °C in ultrahigh vacuum (UHV) for removing the surface contaminants caused by air exposure. Gd_2O_3 and Y_2O_3 epitaxial films with different thicknesses were then e-beam deposited on the GaN (0001) surface using powder-packed and sintered Gd_2O_3 and Y_2O_3 sources, not elemental sources plus oxygen, with a substrate temperature held at 700 and 660 °C, respectively. In-situ reflection high-energy electron diffraction (RHEED) was employed to monitor the crystallographic structure of both the substrate surface and the oxide films prior to and during the oxide deposition.

More detailed structural investigations were carried out by X-ray diffraction with synchrotron radiation at wiggler beamline BL17B of the National Synchrotron Radiation Research Center (NSRRC), Hsinchu, Taiwan. The incident X-rays were monochromatized to an energy of 10 keV by a Si (111) double-crystal monochromator. With two pairs of slits between sample and detector, the typical resolution was set to about 5×10^{-3} Å^{-1}.

An FEI Tecnai F-20 STEM/TEM with a field emission gun operated at 200 kV was used for acquiring STEM-EELS spectra. The size of the electron probe was ∼0.2 nm. The energy resolution of the EELS was 0.63 eV, which was derived from the full-width half-maximum (fwhm) of the zero loss peak.

RESULTS AND DISCUSSION

RHEED patterns during the oxide growth were taken along GaN $\langle 11\bar{2}0\rangle$ and $\langle 10\bar{1}0\rangle$, respectively. The RHEED pattern of the starting GaN surface was a streaky reconstructed (2 × 2). With the Gd_2O_3 thickness larger than 0.8 nm, the patterns turned to a streaky (1 × 1), and with the thickness increasing to more than 5 nm, a reconstructed (3 × 2) appeared, which remained unvaried all the way to 20 nm.[28] The patterns remained streaky during the growth, indicating a two-dimensional (2D) growth. From the systematic X-ray diffraction study as will be discussed later, the initial growth of Gd_2O_3 has yielded a hexagonal phase with surface normal (0001) and in-plane axes of Gd_2O_3 being parallel to the corresponding axes of GaN.

The X-ray diffraction scans along the surface normal of the Gd_2O_3 samples with different oxide thicknesses are shown in Figure 1. The intense sharp peaks of GaN (0002), GaN (0004),

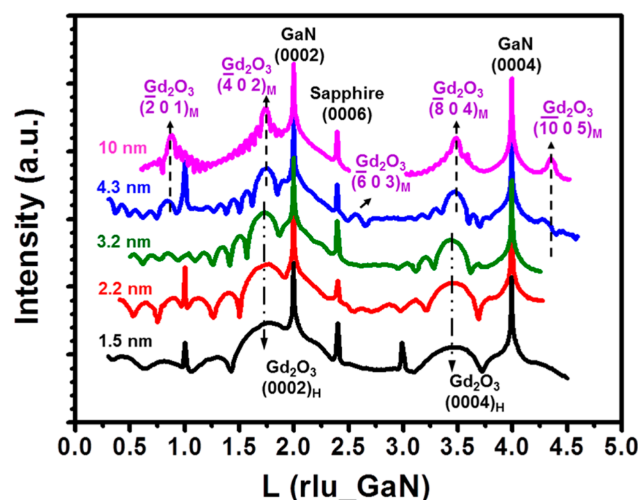

Figure 1. XRD longitudinal scans along surface normal of samples with different Gd_2O_3 layer thickness.

and sapphire (0006) reflections are, respectively, centered at 2.0, 4.0, and 2.395 rlu_{GaN}, the reciprocal lattice unit of GaN along its *c*-axis with 1 $rlu_{GaN} = 2\pi/c_{GaN} = 1.212$ Å^{-1}. The oxide peaks are those with the periodic thickness fringes, which are caused by the interference between the X-rays reflected by the top surface and buried interface. The presence of the pronounced fringes revealed a very smooth surface/interface and good crystalline quality of the Gd_2O_3 epitaxial layer on GaN.

For Gd_2O_3 films with thicknesses of 1.5, 2.2, and 3.2 nm, aside from the main substrate signals, two broad oxide peaks were centered at ∼1.73 and ∼3.44 rlu_{GaN}. The broadness came from the short structural coherence length limited by the small layer thickness. The interplanar spacing corresponding to these peaks was close to that of monoclinic phase $(\bar{4}02)_M$, $(\bar{8}04)_M$ and hexagonal phase $(0002)_H$, $(0004)_H$ planes; it would be very difficult to assign phases based on the observed reflections alone.[28] However, for thicker Gd_2O_3 films of 4.3 and 10 nm, two additional peaks centered at ∼0.87 and ∼2.61 rlu_{GaN} were found. On the basis of JCPDS cards (No. 42-1465),[30] these latter two peaks correspond to $(\bar{2}01)_M$ and $(\bar{6}03)_M$ reflections, and no allowed reflection belonging to the hexagonal phase exists in the nearby region. The absence of these two peaks in the films less than ∼4 nm thick, therefore, indicates that the thinner Gd_2O_3 films have a hexagonal structure. The two oxide peaks of the three thinnest oxide layers were then indexed as the $(0002)_H$ and $(0004)_H$ reflections of the H−Gd_2O_3. For oxide films with thickness above 4 nm, the broad peaks centered at 0.87, 1.75, 2.61, 3.48, and 4.35 rlu_{GaN} were indexed as $(\bar{2}01)_M$, $(\bar{4}02)_M$, $(\bar{6}03)_M$, $(\bar{8}04)_M$ and $(\bar{10}05)_M$ reflections of M−Gd_2O_3, respectively.

The scans along surface normal alone would not provide the off-normal crystallographic information, which is needed for accurately determining the symmetry of the oxide films and the

dx.doi.org/10.1021/am302881y | ACS Appl. Mater. Interfaces 2013, 5, 1436−1441

alignment between the oxides and the substrates. Lateral radial scans were thus performed along the GaN in-plane $\langle 11\bar{2}0\rangle_H$ direction, shown in Figure 2. The measurements were performed in the grazing incidence diffraction geometry by keeping the surface normal almost perpendicular to the vertical scattering plane. For the Gd_2O_3 layers of thickness less than 4 nm, in addition to the narrow GaN $(11\bar{2}0)$ reflection centered at 1 rlu_{GaN}, the reciprocal lattice unit of GaN along the lateral direction with the magnitude of $4\pi/(\sqrt{3}a_{GaN})$ = 2.274 Å^{-1}, a broad peak appears at 0.855 rlu_{GaN}. Both peaks exhibit 6-fold symmetry in azimuthal ϕ scans against the surface normal (not shown), revealing the hexagonal crystalline structure. The broad peak was indexed as the H−Gd_2O_3 $(11\bar{2}0)_H$ reflection, which is aligned with the GaN $(11\bar{2}0)$ reflection. For the samples with Gd_2O_3 thickness greater than 4 nm, the oxide peak splits into two broad peaks, centered at 0.835 and 0.88 rlu_{GaN}, respectively. Even though their azimuthal scans also have six evenly spaced peaks, each peak further splits (not shown). The observed 6-fold symmetry and peak splitting can be accounted for by the coexistence of six rotational domains of M−Gd_2O_3 with $(\bar{2}01)_M$ normal, and each domain has its $[020]_M$ axis aligned with one of the 6-fold symmetric GaN $\langle 11\bar{2}0\rangle$ direction.[28] The two peaks at 0.835 and 0.88 rlu_{GaN} in Figure 2 are indexed as $(3 \pm 13)_M$ and $(0 \pm 20)_M$, respectively.

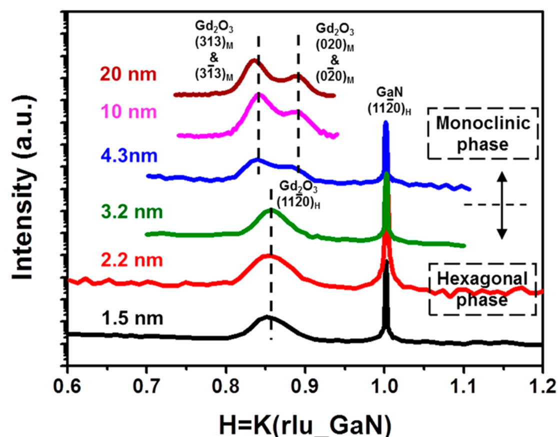

Figure 2. Intensity distributions of in-plane radial scans along GaN $[11\bar{2}0]_H$ direction for Gd_2O_3 samples with thicknesses from 1.5 to 20 nm.

To further verify the crystalline structure of the hetero-epitaxial system, we performed reciprocal space mapping (RSM) around the Gd_2O_3 $(1\bar{1}01)_H$ reflection in the GaN $h-l$ plane. A clean oval-shape peak was obtained from the thin layers with thickness less than 4 nm, as illustrated in Figure 3a−c, indicating that H−Gd_2O_3 possesses only one domain. The reduction in the profile elongation along the l direction reflects the increase of vertical structural coherence length associated with the increasing layer thickness. As the thickness increases beyond 4 nm, the peak profile gradually evolves into a cluster of four peaks. According to the model of $(\bar{2}01)_M$ oriented M−Gd_2O_3 with six rotational domains, the four maxima in the RSM shown in Figure 3d−f are associated with the Gd_2O_3 $(\bar{4}0\bar{1})_M$, $(\bar{3} \pm 10)_M$, $(\bar{1} \pm 12)_M$, and $(003)_M$ reflections, in the order of increasing l value, belonging to six different rotational domains.[28] The evolution of the Gd_2O_3 reflection from a single maximum to four peaks in the RSM shown in Figure 3 as the oxide thickness increases attest the structural transition from

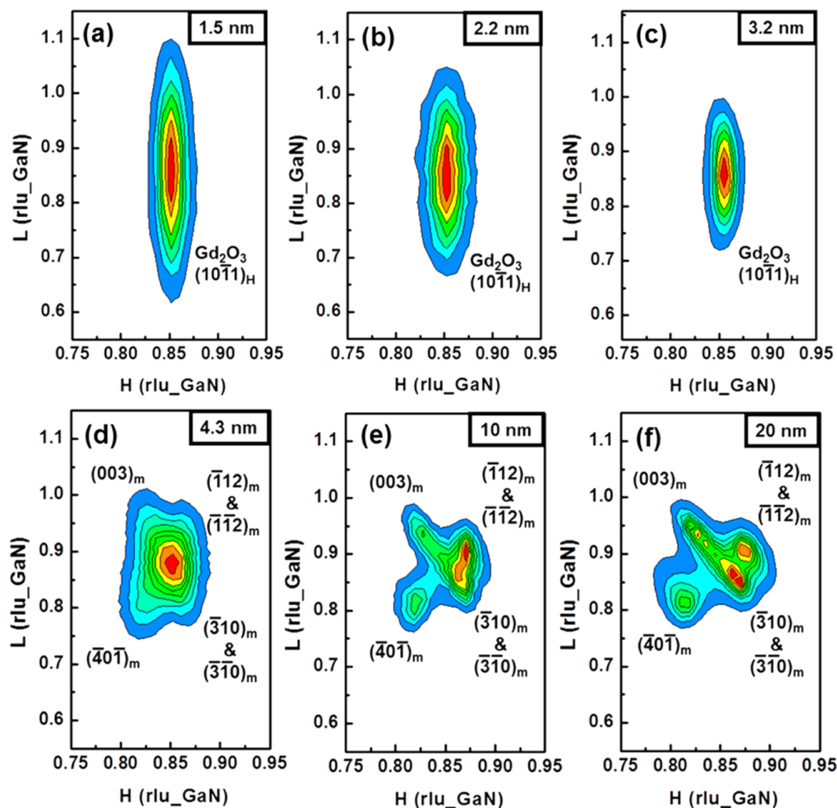

Figure 3. Two-dimensional reciprocal space maps in the GaN $h-l$ plane near the Gd_2O_3 $(10\bar{1}1)_H$ reflection for the samples with a (a) 1.5, (b) 2.2, (c) 3.2, (d) 4.3, (e) 10, and (f) 20 nm thick Gd_2O_3 epilayer.

dx.doi.org/10.1021/am302881y | ACS Appl. Mater. Interfaces 2013, 5, 1436−1441

the hexagonal to the monoclinic phase and the critical thickness is approximately 4 nm.

By fitting the angular positions of many reflections, we derived the lattice parameters of the hexagonal phase to be $a = b = 3.75$ Å and $c = 5.94$ Å, similar to the results of ab initio energetic calculations based on the density functional theory (DFT) and projector augmented wave (PAW) pseudopotentials method.[31] Similarly, the monoclinic phase lattice constants are determined to be $a = 13.965$ Å, $b = 3.595$ Å, $c = 8.787$ Å, and $\beta = 101.34°$. According to the phase diagram, bulk Gd_2O_3 exists in three polymorphic forms: cubic ($Ia\overline{3}$), monoclinic ($C2/m$), and hexagonal ($P\overline{3}m$l) at temperatures below ∼2500 K, and the cubic phase with the bixbyite structure is the one stable at the ambient condition.[32] Both the cubic and monoclinic phases have been reported as existing at room temperatures.[32−34] The hexagonal phase only exists at high pressure or high temperature. It is thus difficult to accurately determine the strain state of the hexagonal phase oxide layers because of the lack of ambient condition data to compare with. Nevertheless, the lattice parameters of H−Gd_2O_3 layer remained practically unchanged and their values are close to the theoretic prediction, implying the lattice is nearly fully relaxed.

Electron-energy loss near edge structure (ELNES) is sensitive to the electronic structure and atomic bonding of the excited element and its shape can be adopted as the fingerprint to differentiate among various atomic structure of a material. In order to further verify the structure of the Gd_2O_3 layers, the ELNES spectra at Gd $N_{4,5}$-edge, shown in Figure 4, and O K-edge, shown in Figure 5, were collected from the 3 nm-thick H−Gd_2O_3 and the 20 nm-thick M−Gd_2O_3 films. Electron beam with a size of 0.2 nm was focused in the oxide layer as marked by the dots on the TEM cross-sectional images shown in the insets of Figure 4. The ELNES spectrum of Gd $N_{4,5}$-edge is associated with electronic transitions from the occupied 4d states to the unoccupied 4f states. Because the 4f electron is located in the inner core level and cannot overlap with ligand orbitals, it does not participate in bonding significantly. Therefore, the Gd $N_{4,5}$ spectra, which are composed of a main peak around 149 eV and pre-edge peaks arising from the multiple transitions between 135 and 145 eV, are insensitive to the bonding between Gd and O and exhibit the similar features for the two samples.

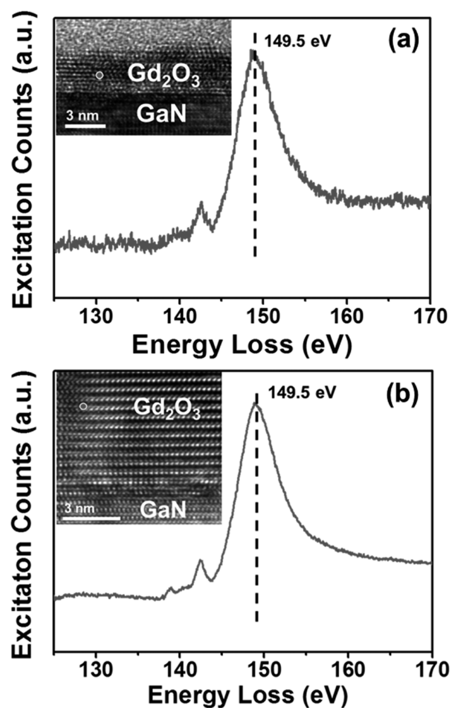

Figure 4. Gd $N_{4,5}$-edges ELNES spectra collected from the (a) 3 nm thick H−Gd_2O_3 layer and (b) 20 nm thick M−Gd_2O_3 layer grown on GaN with the collection semiangle of 10.5 mrad.

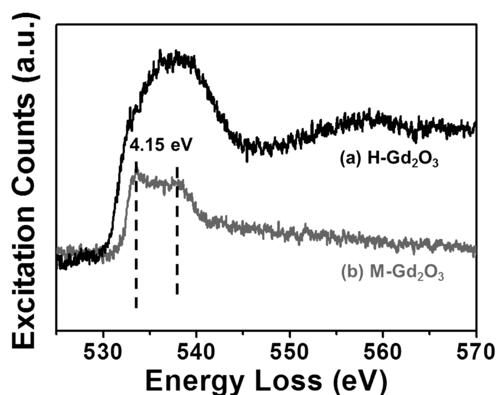

Figure 5. O K-edge ELNES spectra collected from the thin (a) H−Gd_2O_3 and thick (b) M−Gd_2O_3 layers with collection semiangle of 14.6 mrad.

On the other hand, the O K-edge is associated with the direct transitions from O 1s to 2p states and is sensitive to the empty O 2p density of states. In rare earth oxides, these states are mainly mixed with the rare earth 5d states. The obtained O K-edge spectra of the thin and thick films, respectively illustrated by curves a and b in Figure 5, exhibit obvious differences. The ELNES spectrum of M−Gd_2O_3 shows two separate peaks with a 4.15 eV separation. The values of peak separation depends on the crystal structure and the radius of cation for rare earth oxides and can be interpreted in terms of crystal field theory.[35,36] The separate peaks observed in the thick film are attributed to the unoccupied hybridized orbitals [Gd 5d + O 2pπ] and [Gd 5d + O 2pσ] due to the strong hybridization between Gd 5d and oxygen 2p orbitals.[37] In contrast, the separate peaks feature became less evident in the spectrum of the thin film with the hexagonal structure. Only one broad peak was observed and this is consistent with the reported characteristics of hexagonal phase of rare earth sesquioxides.[38]

By applying pressure, the structure of bulk Gd_2O_3 undergoes a series of transition from cubic to monoclinic and then to hexagonal.[32,39] For films of thickness less than ∼4 nm grown on c-plane GaN, Gd_2O_3 appears in the energetically less favorable hexagonal phase, which is stabilized by epitaxy. The epitaxial relationship follows Gd_2O_3 (0001)||GaN (0001) with in-plane axes locking. As the thickness further increases, the structure of the oxide layer transforms into the monoclinic phase with six rotational domains and relative orientation of Gd_2O_3 ($\overline{2}$01)||GaN (0001). The monoclinic phase of Gd_2O_3 can be described as a collective deformation of the hexagonal one subjected to a shear distortion and the $(0001)_H$ axis is tilted by ∼3.7° toward the $[1\overline{1}00]_H$ direction. The high degree of similarity in the atomic arrangement of the two phases indicates that the structural phase transition belongs to the displacive one, which is driven by minimizing the total energy of the epi-layers. Comparing H−Gd_2O_3 with M−Gd_2O_3, H−Gd_2O_3 has a smaller molar volume; thus yielding a higher dielectric constant

dx.doi.org/10.1021/am302881y | ACS Appl. Mater. Interfaces 2013, 5, 1436−1441

of ∼24.[26] The excellent thermal stability of both H−Gd_2O_3 and M−Gd_2O_3 of a few nanometers thick on GaN with high-temperature 1100 °C annealing has been achieved.[26,27] The epitaxial growth of hexagonal and monoclinic Gd_2O_3 on GaN is in strong contrast to that of cubic phase on GaAs[6] and Si.[12,13] Moreover, the H−Gd_2O_3 dielectric is more desirable than its monoclinic counterpart for the role of gate dielectric in inversion-channel GaN MOSFETs due to its single-domain characteristics and higher dielectric constant. Knowing the trend of Gd_2O_3 phase transformation helps the crystal growers to retain the single-domain H−Gd_2O_3 with a precise control in the oxide thickness. It is noteworthy that identical structure and epitaxial relationship were observed on Y_2O_3 grown on *c*-plane GaN. The same hexagonal to monoclinic structure transition occurred at a slightly smaller critical thickness, ∼3 nm. An increase of dielectric constant accompanying the structure transition was also observed.[28] The excellent thermal and electrical properties of the epitaxy stabilized ultrathin hexagonal Gd_2O_3 and Y_2O_3 films strongly favor their application as gate dielectrics for advanced GaN MOS.

■ CONCLUSION

Gd_2O_3 and Y_2O_3 epilayers on GaN (0001) have the hexagonal phase with their thickness less than a critical value t_c (3−4 nm), as stabilized by epitaxy. The hexagonal to monoclinic phase transition occurs as thickness exceeds t_c. The stabilization of the single-domain hexagonal phase at a few nanometers thick with high thermal stability, a high dielectric constant, and a low interfacial density of states strongly favors the application of single crystal Gd_2O_3 and Y_2O_3 as gate dielectrics for advanced GaN MOS devices with low EOT.

■ AUTHOR INFORMATION

Corresponding Author

*E-mail: chsu@nsrrc.org.tw (C.-H.H.); mhong@phys.ntu.edu.tw (M.H.).

Author Contributions

⊥These authors have made equal contributions to this work.

Notes

The authors declare no competing financial interest.

■ ACKNOWLEDGMENTS

The authors wish to thank the National Science Council, Taiwan, under grants of NSC-101-2120-M-002-016 and NSC-99-2119-M-007-006-MY3, and the Asian Office of Aerospace Research and Development of the US Air Force for supporting this work. The experiment on ELNES was carried out at the lab of Prof. C. H. Chen and Dr. M. W. Chu of CCMS, National Taiwan University, and we thank them for their help.

■ REFERENCES

(1) In *Condensed-Matter Physics, Physics through the 1990s*; National Research Council, The National Academies Press: Washington, DC, 1986.

(2) Kwo, J.; Hong, M.; Nakahara, S. *Appl. Phys. Lett.* **1986**, *49*, 319−321.

(3) Nakamura, S.; Mukai, T.; Senoh, M. *Appl. Phys. Lett.* **1994**, *64*, 1687−1689.

(4) Egawa, T.; Zhang, B.; Ishikawa, H. *IEEE Electron Device Lett.* **2005**, *26*, 169−171.

(5) Iwakami, S.; Machida, O.; Yanagihara, M.; Ehara, T.; Kaneko, N.; Goto, H.; Iwabuchi, A. *Jpn. J. Appl. Phys.* **2007**, *46*, L587−L589.

(6) Hong, M.; Kwo, J.; Kortan, A. R.; Mannaerts, J. P.; Sergent, A. M. *Science* **1999**, *283*, 1897−1900.

(7) Nozaki, T.; Hirohata, A.; Tezuka, N.; Sugimoto, S.; Inomata, K. *Appl. Phys. Lett.* **2005**, *86*, 082501.

(8) Lin, B. H.; Liu, W. R.; Yang, S.; Kuo, C. C.; Hsu, C.-H.; Hsieh, W. F.; Lee, W. C.; Lee, Y. J.; Hong, M.; Kwo, J. *Cryst. Growth Des.* **2011**, *11*, 2846−2851.

(9) Ren, F.; Hong, M. W.; Hobson, W. S.; Kuo, J. M.; Lothian, J. R.; Mannaerts, J. P.; Kuo, J.; Chen, Y. K.; Cho, A. Y. Enhnacement-Mode p-Channel GaAs MOSFETs on Semi-Insulating Substrates. *IEEE International Electron Devices Meeting*, San Francisco, Dec 8−11, 1996; pp 943−945.

(10) Kuhn, K. J. *IEEE T. Electron Dev.* **2012**, *59*, 1813−1828.

(11) International Technology Roadmap for Semiconductor 2011 edition. http://www.itrs.net/Links/2011ITRS/Home2011.htm. (Accessed January 24, 2013).

(12) Lin, T. D.; Hang, M. C.; Hsu, C. H.; Kwo, J.; Hong, M. *J. Cryst. Growth* **2007**, *301*−*302*, 386−389.

(13) Kwo, J.; Hong, M.; Kortan, A. R.; Queeney, K. T.; Chabal, Y. J.; Mannaerts, J. P.; Boone, T.; Krajewski, J. J.; Sergent, A. M.; Rosamilia, J. M. *Appl. Phys. Lett.* **2000**, *77*, 130−132.

(14) Molle, A.; Wiemer, C.; Bhuiyan, M. N. K.; Tallarida, G.; Fanciulli, M.; Pavia, G. *Appl. Phys. Lett.* **2007**, *90*, 193511.

(15) Sowwan, M.; Yacoby, Y.; Pitney, J.; MacHarrie, R.; Hong, M.; Cross, J.; Walko, D. A.; Clarke, R.; Pindak, R.; Stern, E. A. *Phys. Rev. B* **2002**, *66*, 205311.

(16) Kwo, J.; Hong, M.; Kortan, A. R.; Queeney, K. L.; Chabal, Y. J.; Opila, R. L.; Muller, D. A.; Chu, S. N. G.; Sapjeta, B. J.; Lay, T. S.; Mannaerts, J. P.; Boone, T.; Krautter, H. W.; Krajewski, J. J.; Sergnt, A. M.; Rosamilia, J. M. *J. Appl. Phys.* **2001**, *89*, 3920−3927.

(17) Molle, A.; Perego, M.; Bhuiyan, Md. N. K.; Wiemer, C.; Tallarida, G.; Franciulli, M. *J. Appl. Phys.* **2007**, *102*, 034513.

(18) Morkoc, H.; Strite, S.; Gao, G. B.; Lin, M. E.; Sverdlov, B.; Burns, M. *J. Appl. Phys.* **1994**, *76*, 1363−1398.

(19) Irokawa, Y.; Nakano, Y.; Ishiko, M.; Kachi, T.; Kim, J.; Ren, F.; Gila, B. P.; Onstine, A. H.; Abernathy, C. R.; Pearton, S. J.; Pan, C.-C.; Chen, G.-T.; Chyi, J.-I. *Appl. Phys. Lett.* **2004**, *84*, 2919−2921.

(20) Lee, K. T.; Huang, C. F.; Gong, J.; Lee, C. T. *IEEE Electron Device Lett.* **2011**, *32*, 306−308.

(21) Chang, Y. C.; Chang, W. H.; Chiu, H. C.; Tung, L. T.; Lee, C. H.; Shiu, K. H.; Hong, M.; Kwo, J.; Hong, J. M.; Tsai, C. C. *Appl. Phys. Lett.* **2008**, *93*, 053504.

(22) Chang, Y. C.; Chang, W. H.; Chang, Y. H.; Kwo, J.; Lin, Y. S.; Hsu, S. H.; Hong, J. M.; Tsai, C. C.; Hong, M. *Microelectron. Eng.* **2010**, *87*, 2042−2045.

(23) Ren, F.; Hong, M.; Chu, S. N. G.; Marcus, M. A.; Schurman, M. J.; Baca, A.; Pearton, S. J.; Abernathy, C. R. *Appl. Phys. Lett.* **1998**, *73*, 3893−3895.

(24) Matocha, K.; Chow, T. P.; Gutmann, R. J. *IEEE T. Electron Dev.* **2005**, *52*, 6−10.

(25) Hong, M.; Kwo, J.; Chu, S. N. G.; Mannaerts, J. P.; Kortan, A. R.; Ng, H. M.; Cho, A. Y.; Anselm, K. A.; Lee, C. M.; Chyi, J. I. *J. Vac. Sci. Technol. B* **2002**, *20*, 1274−1277.

(26) Chang, W. H.; Lee, C. H.; Chang, Y. C.; Chang, P.; Huang, M. L.; Lee, Y. J.; Hsu, C. H.; Hong, J. M.; Tsai, C. C.; Kwo, J.; Hong, M. *Adv. Mater.* **2009**, *21*, 4970−4974.

(27) Chang, W. H.; Lee, C. H.; Chang, P.; Chang, Y. C.; Lee, Y. J.; Kwo, J.; Tsai, C. C.; Hong, J. M.; Hsu, C. -H.; Hong, M. *J. Cryst. Growth* **2009**, *311*, 2183−2186.

(28) Chang, W. H.; Chang, P.; Lai, T. Y.; Lee, Y. J.; Kwo, J.; Hsu, C. -H.; Hong, M. *Cryst. Growth Des.* **2010**, *10*, 5117−5122.

(29) Chang, W. H.; Chang, P.; Lee, W. C.; Lai, T. Y.; Kwo, J.; Hsu, C. -H.; Hong, J. M.; Hong, M. *J. Cryst. Growth* **2011**, *323*, 107−110.

(30) JCPDS cards (No. 42-1465).

(31) Wu, B.; Zinkevich, M.; Aldinger, F.; Wen, D.; Chen, L. *J. Solid State Chem.* **2007**, *180*, 3280−3287.

(32) Zinkevich, M. *Prog. Mater. Sci.* **2007**, *52*, 597−647.

(33) Warshaw, I.; Roy, R. *J. Phys. Chem.* **1961**, *65*, 2048−2051.

(34) Sato, S.; Takahashi, R.; Kobune, M.; Gotoh, H. *Appl. Catal. A–Gen.* **2009**, *356*, 57–63.
(35) Wang, X. F.; Li, Q.; Moreno, M. S. *J. Appl. Phys.* **2008**, *104*, 093529.
(36) Pailloux, F.; Jublot, M.; Gaboriaud, R. J.; Jaouen, M.; Paumier, F. *Phys. Rev. B* **2005**, *72*, 125425.
(37) Baeck, J. H.; Park, S. A.; Lee, W. J.; Jeong, I. S.; Jeong, K.; Cho, M.-H.; Kim, Y. K.; Min, B. G.; Ko, D. H. *J. Chem. Phys.* **2009**, *130*, 204510.
(38) Calmels, L.; Coulon, P. E.; Schamm-Chardon, S. *Appl. Phys. Lett.* **2011**, *98*, 243116.
(39) Lonappan, D.; Shekar, N. V. C.; Sahu, P. C.; Kumarasamy, B. V.; Bandyopadhyay, A. K.; Rajagopalan, M. *Phil. Mag. Lett.* **2008**, *88*, 473–479.